Structure of 3,4-Dihydroxy-2-butanone 4-Phosphate Synthase from *Methanococcus jannaschii* in Complex with Divalent Metal Ions and the Substrate Ribulose 5-Phosphate

IMPLICATIONS FOR THE CATALYTIC MECHANISM*

Stefan Steinbacher‡§, Susanne Schiffmann¶, Gerald Richter¶, Robert Huber‡, Adelbert Bacher¶, and Markus Fischer¶

From the ‡Max-Planck-Institut für Biochemie, Abteilung für Strukturforschung, Am Klopferspitz 18a, D-82152 Martinsried and the ¶Lehrstuhl für Organische Chemie und Biochemie, Technische Universität München, Lichtenbergstrasse 4, D-85747 Garching, Germany

Skeletal rearrangements of carbohydrates are crucial for many biosynthetic pathways. In riboflavin biosynthesis ribulose 5-phosphate is converted into 3,4-dihydroxy-2-butanone 4-phosphate while its C4 atom is released as formate in a sequence of metal-dependent reactions. Here, we present the crystal structure of *Methanococcus jannaschii* 3,4-dihydroxy-2-butanone 4-phosphate synthase in complex with the substrate ribulose 5-phosphate at a dimetal center presumably consisting of non-catalytic zinc and calcium ions at 1.7-Å resolution. The carbonyl group (O2) and two out of three free hydroxyl groups (OH3 and OH4) of the substrate are metal-coordinated. We correlate previous mutational studies on this enzyme with the present structural results. Residues of the first coordination sphere involved in metal binding are indispensable for catalytic activity. Only Glu-185 of the second coordination sphere cannot be replaced without complete loss of activity. It contacts the C3 hydrogen atom directly and probably initiates enediol formation in concert with both metal ions to start the reaction sequence. Mechanistic similarities to Rubisco acting on the similar substrate ribulose 1,5-diphosphate in carbon dioxide fixation as well as other carbohydrate (reducto-) isomerases are discussed.

Riboflavin (vitamin B_2) is biosynthesized in plants and numerous microorganisms but not in animals, which depend on nutritional sources. Its derivatives, flavin mononucleotide (FMN) and flavinadenine dinucleotide (FAD), are indispensable in all cells where they serve a variety of redox reactions (1). They have also been shown to serve a variety of other functions in cells such as DNA photorepair (2), light sensing (3, 4), and bioluminescence (5–8) and in reactions without net-redox change (9).

Gram-negative bacteria are absolutely dependent on endogenous synthesis of riboflavin, because they are devoid of an uptake system for flavins or flavocoenzymes. Hence, riboflavin-deficient mutants *e.g.* of *Escherichia coli* and *Salmonella* sp. require extremely high concentrations of exogenous riboflavin for growth. The same is true for yeasts such as *Saccharomyces cerevisiae* and *Candida guilliermondii* (for review see Refs. 1 and 10–13). Thus, these organisms should be vulnerable to inhibitors of the riboflavin biosynthesis, which could therefore qualify as novel anti-infective agents. The absence of the riboflavin pathway in the human host appears advantageous in this context, because host/parasite selectivity of inhibitory agents would not constitute a problem. The mechanistic and structural analysis of the riboflavin pathway could serve as the basis for the rational design of riboflavin pathway inhibitors.

3,4-Dihydroxy-2-butanone 4-phosphate synthase supplies the building blocks for the assembly of the xylene ring of the vitamin (14–17). In fact, all eight carbon atoms of the xylene moiety are derived from the product of the enzyme. In the biosynthetic pathway, 3,4-dihydroxy-2-butanone 4-phosphate is condensed with 5-amino-6-ribitylamino-2,4(1*H*,3*H*)-pyrimidinedione derived from GTP (14, 17–26). The reaction product, 6,7-dimethyl-8-ribityllumazine, undergoes a highly unusual dismutation catalyzed by riboflavin synthase, which involves the exchange of a 4-carbon fragment between two identical substrate molecules. The dismutation affords riboflavin and 5-amino-6-ribitylamino-2,4(1*H*,3*H*)-pyrimidinedione, which is recycled as a substrate of 6,7-dimethyl-8-ribityllumazine synthase (27–29).

The reaction catalyzed by 3,4-dihydroxy-2-butanone 4-phosphate synthase involves the release of carbon atom 4 of the substrate, ribulose 5-phosphate, as formate (14, 16, 30) (Fig. 1). Moreover, the position 1-hydroxy group of the substrate is removed. The overall reaction affords a 1-deoxytetrulose phosphate (*DHBP* in Fig. 1) from the pentulose phosphate substrate (Ru5P).[1] Mechanistic studies suggest that the reaction is initiated by the formation of the endiol **1**, which resembles a postulated intermediate of ribulose-diphosphate carboxylase (Rubisco) (31–33). Protonation of the position 1-hydroxy group could then be conducive to the formation of the hypothetical diketone **4** via the enol **3**. A sigmatropic rearrangement could afford the branched carbohydrate **5**, which could subsequently

The atomic coordinates and structure factors (code 1PVW and 1PVY) have been deposited in the Protein Data Bank, Research Collaboratory for Structural Bioinformatics, Rutgers University, New Brunswick, NJ (http://www.rcsb.org/).

§ To whom correspondence should be addressed: Division of Chemistry and Chemical Engineering, Mail Code 114-96, California Institute of Technology, Pasadena, CA 91125. Tel.: 626-395-2662; Fax: 626-744-9524; E-mail: steinbac@caltech.edu.

[1] The abbreviations used are: Ru5P, ribulose 5-phosphate; RuBP, ribulose 1,5-diphosphate; DBPS, 3,4-dihydroxy 2-butanone 4-phosphate synthase; Rubisco, ribulose-diphosphate carboxylase; IspC, 1-deoxy-D-xylulose 5-phosphate reductoisomerase; r.m.s., root mean square.
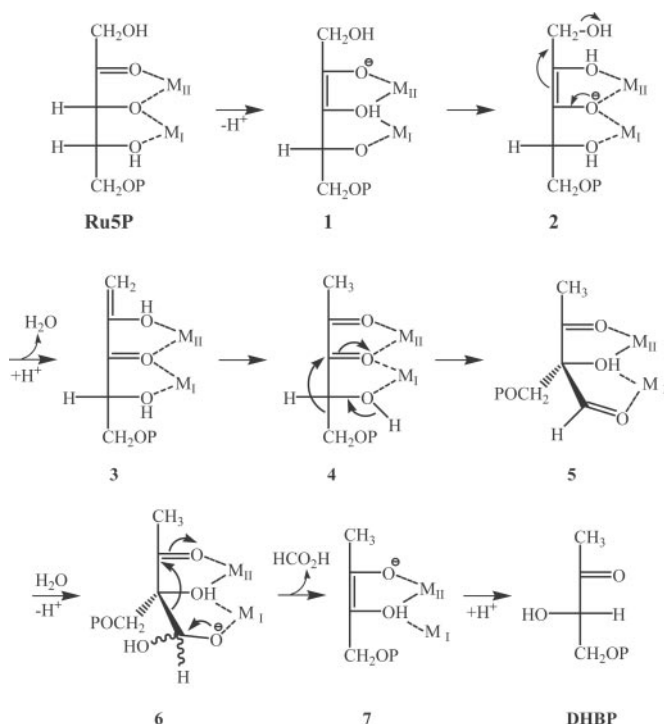
F<small>IG</small>. 1. **Reaction performed by 3,4-dihydroxy 2-butanone 4-phosphate synthase (DBPS).** Ru5P is bound to two divalent metal ions (compare with Fig. 3*a*). The diketone **4** can also be generated by a side reaction of Rubisco mutants (compare with Fig. 6). For details see text.

fragment under formation of the endiol **7**, which could afford the enzyme product, 3,4-dihydroxy-2-butanone 4-phosphate.

The structure of *Escherichia coli* 3,4-dihydroxy-2-butanone 4-phosphate synthase has been determined by x-ray crystallography (34) and by NMR spectroscopy (35). A fortuitous complex of the enzyme from *Magnaporthe grisea* with glycerol used as cryoprotectant helped to define the active site (36), but the details of the enzyme-catalyzed reaction trajectory are still insufficiently understood. This report describes the structure of 3,4-dihydroxy-2-butanone 4-phosphate synthase of the archaebacterium *Methanococcus jannaschii* in complex with the substrate ribulose 5-phosphate and divalent metals defining the enzyme substrate complex at near-atomic resolution.

MATERIALS AND METHODS

Crystallization and Data Collection—Recombinant *M. jannaschii* DBPS was purified as described previously (30) and concentrated to about 30 mg ml^{-1} in 350 mM potassium phosphate, pH 7.2. Prior to crystallization 2 mM ZnCl$_2$ was added, and the buffer was exchanged to 2 mM ZnCl$_2$ and 20 mM Tris/HCl, pH 7.5, by a NAP-10 column. Addition of higher zinc concentrations resulted in precipitation of the enzyme, which could be reversed by addition of zinc-free enzyme or EDTA. Orthorhombic crystals of space group C222(1) containing three monomers in the asymmetric unit (44% solvent content) were obtained from 18% polyethylene glycol 1000, 200 mM calcium (acetate)$_2$, 2 mM ZnCl$_2$, and 0.1 M Tris/HCl, pH 7.5, by mixing 2 μl of the protein solution and 2 μl of the precipitant equilibrated over 300 μl of the reservoir solution at 20 °C in Cryschem plates. Crystals of about 0.4 × 0.3 × 0.3 mm^3 appeared within 1 day with freshly prepared protein. Storage of the protein at 4 °C resulted in significantly impaired crystallization behavior after 1–2 weeks. The mutant His-147 → Ser was crystallized under identical condition as long plates belonging to the monoclinic space group P2(1) with two monomers in the asymmetric unit (40% solvent content), which could be efficiently propagated by macro-seeding. These were transferred in about ten steps into a buffer containing 30% (v/v) polyethylene glycol 400 as cryoprotectant in addition to the components of the reservoir solution.

The Ortho and derivative data sets were collected at 12 °C, whereas the data set Mono was collected at 100 K under cryogenic conditions

using an Oxford cryostream. Derivatives were prepared by soaking orthorhombic crystals for 2 h (Hg and Hg2 with identical soaking conditions) or overnight (Ta, HgTa) in the reservoir solution containing 2 mM thiomersal, saturated Ta$_6$Br$_{14}$ (<1 mM), or both, respectively. All x-ray data were collected on an MARResearch345 image plate detector mounted on a Rigaku RU-200 rotating anode operated at 50 kV and 100 mA with λ (CuKα) = 1.542 Å. Diffraction intensities were integrated and reduced using either the program MOSFLM (37) and the CCP4 suite (37) or the HKL suite (38).

Structure Determination and Refinement—Initial heavy atom positions for the Hg derivative (thiomersal) were identified with the program SHELXS (39), whereas all others were analyzed by the inspection of difference Fourier maps. Heavy atom parameters were refined using MLPHARE (37). Phase calculation was performed between 25- and 3.0-Å resolution for the orthorhombic crystal form. The electron density was improved by solvent flattening using the program DM (37) and 3-fold NCS averaging using the program AVE (40). Tables I and II give a summary of the data collection and phasing statistics.

The 3.0-Å electron density map was of high quality and permitted unambiguous chain tracing of the model in the first round of model building using the program MAIN (41). Refinement steps carried out consisted of conjugate gradient minimization, simulated annealing, and *B*-factor refinement with the program CNS using the mlf target (42). For cross-validation a random test set of 5% of the total number of reflections was excluded from the refinement and used for the calculation of the free *R*-factor (43). The non-crystallographic symmetry restraints were released in the last cycles of refinement for the high resolution data set Mono. The Ramachandran plot (44) calculated with the program PROCHECK (45) showed no residues with angular values in forbidden areas. The coordinates and structure factor amplitudes have been deposited with the Protein Data Bank under accession codes 1PVW and 1PVY.

RESULTS AND DISCUSSION

Structure Solution—Recombinant enzymatically active *M. jannaschii* 3,4-dihydroxy 2-butanone 4-phosphate synthase (DBPS) was crystallized in the orthorhombic space group C222(1) with three monomers in the asymmetric unit. This crystal form was extremely sensitive to buffer changes, and therefore no cryoprotectant could be found. However, crystals were stable enough at room temperature to allow collection of a complete data set to 2.45-Å resolution and the preparation of heavy atom derivatives. The structure was subsequently solved by multiple isomorphous replacement (Tables I and II). The point mutant His-147 → Ser that showed only ~10% of the wild type enzymatic activity yielded a monoclinic crystal form under identical conditions. This crystal form with a dimer in the asymmetric unit was less sensitive to buffer changes and could be soaked with the substrate ribulose 5-phosphate in a suitable cryoprotectant. Diffraction data could be collected at cryogenic conditions to 1.7-Å resolution.

Both structures were refined to crystallographic *R*-factors of 22.9% (R_{free} 28.9%) and 21.3% (R_{free} 25.9%), respectively (Table III). The three monomers of the orthorhombic crystal form showed ordered residues Asn-2 to Tyr-220. In monomer A the acidic active site loop was completely ordered, whereas it has weak side-chain densities for Tyr-20, Glu-24, Arg-25, and Glu-26 in monomer B, and weak side-chain densities for Glu-26 and Glu-28 in monomer C. Asp-30 of the acidic loop is well ordered in all subunits. The acidic active site loops were not engaged in crystal contacts in monomers B and C, but in monomer A the turn region around Asp-23 and Glu-24 had a long van der Waals contact to Arg-201 of a neighboring monomer, however, with distances larger that about 4.5 Å. The active site in monomer A clearly shows two metal and a phosphate ion assembled around His-164 in a well defined dimetal cluster that can be readily interpreted. The other two subunits, however, show extensive broken densities that can not readily be interpreted besides the metal binding to His-164 in accordance with the significant disorder of the acidic active site loop. In addition, residues Lys-109 to Thr-112 (monomer A), residues

TABLE I
Data collection

	Ortho	Mono
Limiting resolution (Å) (last shell)	20–2.45 (2.45–2.54)	20–1.70 (1.70–1.76)
Space group	C222(1)	P2(1)
Unit cell (in Å)	66.3, 154.2, 133.2	53.2, 69.3, 57.1; $\beta = 93.5°$
R_{merge} (last shell)[a]	6.5 (29.5)	6.0 (47.6)
Unique reflections	24,943	42,575
Completeness (last shell)	97.8 (97.3)	93.6 (97.8)
$I/\sigma(I)$ (last shell)	21.5 (3.5)	16.3 (2.4)
Multiplicity	4.7	2.5

[a] $R_{\text{merge}} = \Sigma_{\text{hkl}}[(\Sigma_i |I_i - \langle I \rangle|)/\Sigma_i I_i]$.

TABLE II
Phasing statistics

Data set Ortho was used as the native set. Derivative data sets Hg and Hg2 occupy the same sites. The mean figure of merit was 0.49 in the resolution range 25-3.0 Å.

	Hg	Hg2	Ta	HgTa
Resolution collected (Å)	23–3.2	25–3.0	25–2.5	26–3.0
Unique reflections	10,866	13,866	24,785	14,136
R_{merge}	10.2	8.4	6.9	11.8
R_{iso}[a]	23.5	24.7	9.6	24.0
Resolution used for phasing (Å)	3.2	3.0	5.5	4.5
Number of sites	4	4	3	7
Phasing power[b]	1.96	1.79	1.76	2.49
R_{Cullis}[c]	0.66	0.69	0.67	0.56

[a] $R_{\text{iso}} = \Sigma |F_{\text{PH}} - F_{\text{P}}|/\Sigma F_{\text{P}}$.
[b] Phasing power, $\langle |F_{\text{H}}| \rangle$/r.m.s. lack of closure.
[c] R_{Cullis} = r.m.s. lack of closure/r.m.s. isomorphous differences.

TABLE III
Refinement statistics

	Ortho	Mono
Resolution range (Å)	20.0–2.45	20–1.70
Reflections (working set)	23,705 (93.1%)	40,421 (88.7%)
Reflections (test set)	1,210 (4.8%)	2,141 (4.7%)
R_{cryst} (%)[a]	22.9	21.3
R_{free} (%)[b]	28.9	25.9
Non-hydrogen protein atoms	5,220	3,472
Total number of metal ions	2 zinc, 1 calcium	3 zinc, 4 calcium
Solvent molecules	—	352
B-factors (Å²)		
Protein	43.9	29.3
Solvent	—	36.2
Active site metals	31.3	31.0
Ru5P	—	28.4
r.m.s. deviation		
Bond length (Å)	0.0083	0.0109
Bond angle (°)	1.24	1.48

[a] $R_{\text{cryst}} = \Sigma_{\text{hkl} \subset W} ||F_{\text{abs}}| - k|F_{\text{calc}}||/\Sigma_{\text{hkl} \subset W} |F_{\text{abs}}|$.

[b] $R_{\text{free}} = \Sigma_{\text{hkl} \subset T} ||F_{\text{abs}}| - k|F_{\text{calc}}||/\Sigma_{\text{hkl} \subset T} |F_{\text{abs}}|$.

Tyr-89 to Glu-98 (monomer B), and residues around Tyr-95 (monomer C) are disordered or have very weak electron densities. Although refined without non-crystallographic symmetry restraints, the monomers were very similar showing r.m.s. deviations of only 0.66 Å for 217 Cα atoms (monomer A to B) and 0.40 Å for 218 Cα atoms (monomer A to C), respectively.

The monoclinic crystal form showed ordered residues Asn-2 to Tyr-220 and Asn-3 to Leu-221, respectively, for both asymmetric monomers and 347 solvent molecules. Both monomers showed an r.m.s. deviation of only 0.39 Å for 214 Cα atoms without imposing non-crystallographic symmetry restraints. In addition, each active site had one molecule of ribulose 5-phosphate and two metal ions, presumably zinc and calcium, from the crystallization buffer bound at the active site with each metal ion binding an additional water ligand. The average temperature factors of Ru5P (28.4 Å²) were slightly lower than for the protein (29.3 Å²) and both metal ions 31.0 (Å²) at the active site, which indicates full occupancy and ordering. The Tyr-95 loop is observed in two conformations. The acidic active

site loop from Tyr-20 to Asp-30 was well ordered in both monomers. Calcium and zinc ions were involved in crystal contacts in both crystal forms.

Overall Structure and Active Site Entrance—DBPS from *Escherichia coli* (34), *M. grisea* (36), and *M. jannaschii* (Fig. 2a) form identical homodimers in the crystals, which also reflect the solution state of the enzyme. Each monomer is composed of an $\alpha+\beta$ structure with a rather complex topology for the β-strand connectivity. It has a prominent internal active site cavity mainly formed from one monomer with one side being lined by residues of the neighboring subunit (Thr-112 loop and His-147 loop) (Fig. 2b). This cavity appears open due to the disorder of the acidic active site loop in the absence of metals and substrate (34) but is closed by this loop upon binding of the substrate ribulose 5-phosphate or glycerol in the presence of divalent metals. In addition, the loop around Tyr-95 is observed in two conformations in the asymmetric dimer of the monoclinic crystal form. In an open conformation the Tyr-95 loop points away from the active site, whereas in the closed the

FIG. 2. **Overall structure of *M. jannaschii* DBPS.** *a*, ribbon diagram of the *M. jannaschii* DPBS dimmer. The bound substrate Ru5P is depicted as a *red ball-and-stick model*, with the acidic loop in *purple*. Regions at the active site entrance deviating from the *M. grisea* enzyme, including the Ty-95 loop are shown in *orange* and *light blue*, respectively. *b*, active site entrance. The acidic active site loop is shown in *light blue*. The Tyr-95 loop (*blue* and *orange*) is observed in two conformations in the monoclinic crystal form. The Thr-112 and His-147 (*S147*) loops are contributed from the neighboring subunit.
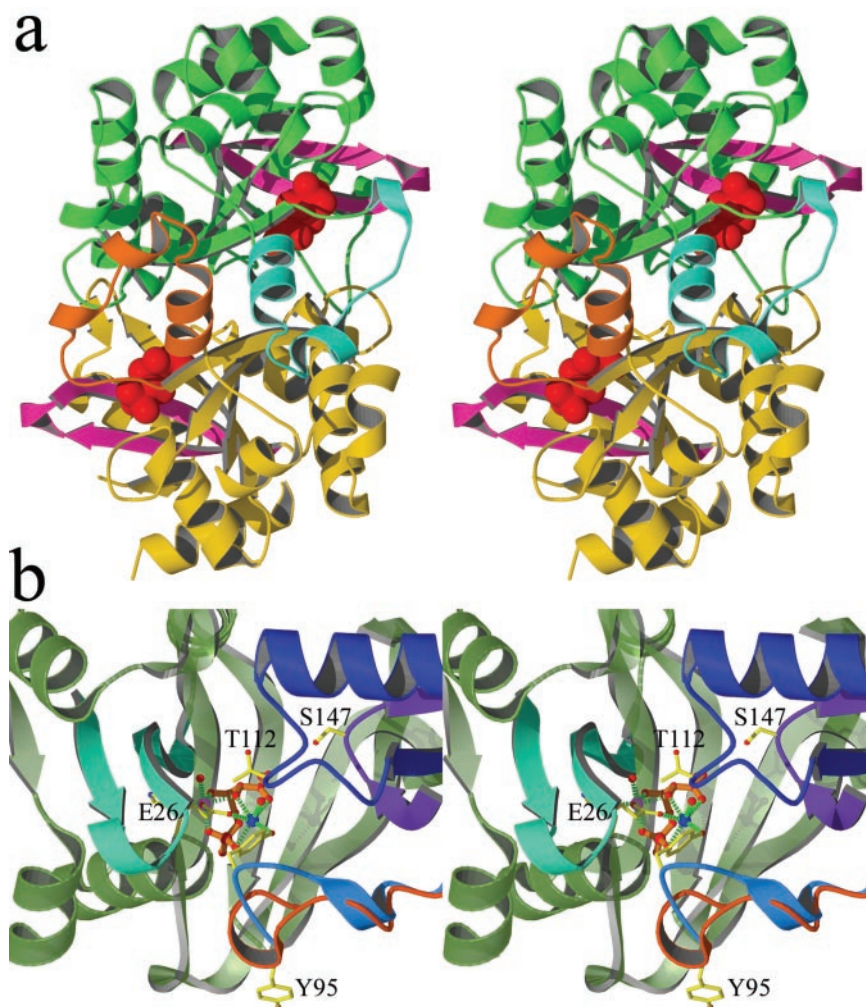
phenolic OH group of Tyr-95 is a direct ligand to metal II. This region is not conserved between different DBPS and is part of an insertion of the *M. jannaschii* enzyme compared with *M. grisea* (30). The Tyr-95 ligand is not essential for the formation of the dimetal center, because it can be replaced by a water molecule. In addition, in the well ordered two-metal center of the orthorhombic crystal form, the Tyr-95 loop is observed in yet another conformation resembling the closed state, however the phenolic OH only hydrogen-bonds to a water molecule on metal II. We conclude that the Tyr-95 loop contributes to active site access in *M. jannaschii* DBPS but is not essential for assembly of the dimetal center. In contrast, the Thr-112 loop and the His-147 loop (which bears the mutation His-147 Ser yielding the monoclinic crystal form) from the neighboring subunit are found in almost identical conformations in all available structures. The same is true for the acidic active site loop in Mn^{2+}·glycerol·sulfate complex of *M. grisea* (36) and the substrate·dimetal complex of the present study. In the absence of substrate this loop may either be completely disordered (34) or it may adopt deviating conformations. The *M. grisea* (36) and the *M. jannaschii* DBPS monomers superimpose with an r.m.s. deviation of 1.22 Å for 171 Cα atoms reflecting this similarity.

Active Site Architecture and Metal-mediated Binding of Ribulose 5-Phosphate—The active site is formed on one side of the central β-sheet of DBPS and the N terminus of the α-helix from Gly-163 to Ala-175, which contributes His-164 as a central active site residue. The acidic active site loop from Val-19 to Asp-30 as well as loop structures around Tyr-95, Thr-112, and His-147 constitute the other parts of the active site (Fig. 2*b*).

Most of these regions reside within one monomer with exception of the loops around Thr-112 and His-147, which belong to the neighboring monomer. Both the available *E. coli* structures (34, 35) and the present study indicate high flexibility at the active site. Ordering of the acidic active site loop is concomitant to binding of two divalent metal ions and a phosphate/sulfate ion or the substrate ribulose 5-phosphate, respectively.

The phosphate moiety of the substrate ribulose 5-phosphate is anchored by four hydrogen bonds (side chain and backbone amide of Thr-165, backbone amide of His-164) and four salt bridge interactions (Arg-25 and Arg-161). In addition, each of the two metal ions is coordinated by a phosphate oxygen (Fig. 3). The carbohydrate chain of ribulose 5-phosphate is fixed by four metal coordination bonds, two of which are formed by zinc (metal I) to O3 and O4 and two by calcium (metal II) to O2 and O3. Only one direct protein substrate interaction is observed between O4 and the side chain of Asp-30 from the acidic loop. The O1 hydroxyl group appears in two conformations and has a somewhat weaker electron density, which can be explained by the lack of direct contacts. Both metal ions show one water ligand in addition to the protein and substrate contacts. A prominent water molecule is found near O3 that is coordinated by Glu-28 of the acidic loop and Glu-185.

DBPS proteins of different organisms have been shown to require Mg^{2+} or Mn^{2+} for catalytic activity. The previous structural characterization of the *M. grisea* DBPS (36) provides insight into metal binding in the presence of sulfate ions. Mg^{2+} and Mn^{2+} can assemble into a dimetal center in the presence of sulfate in a geometry that is very similar to that observed for
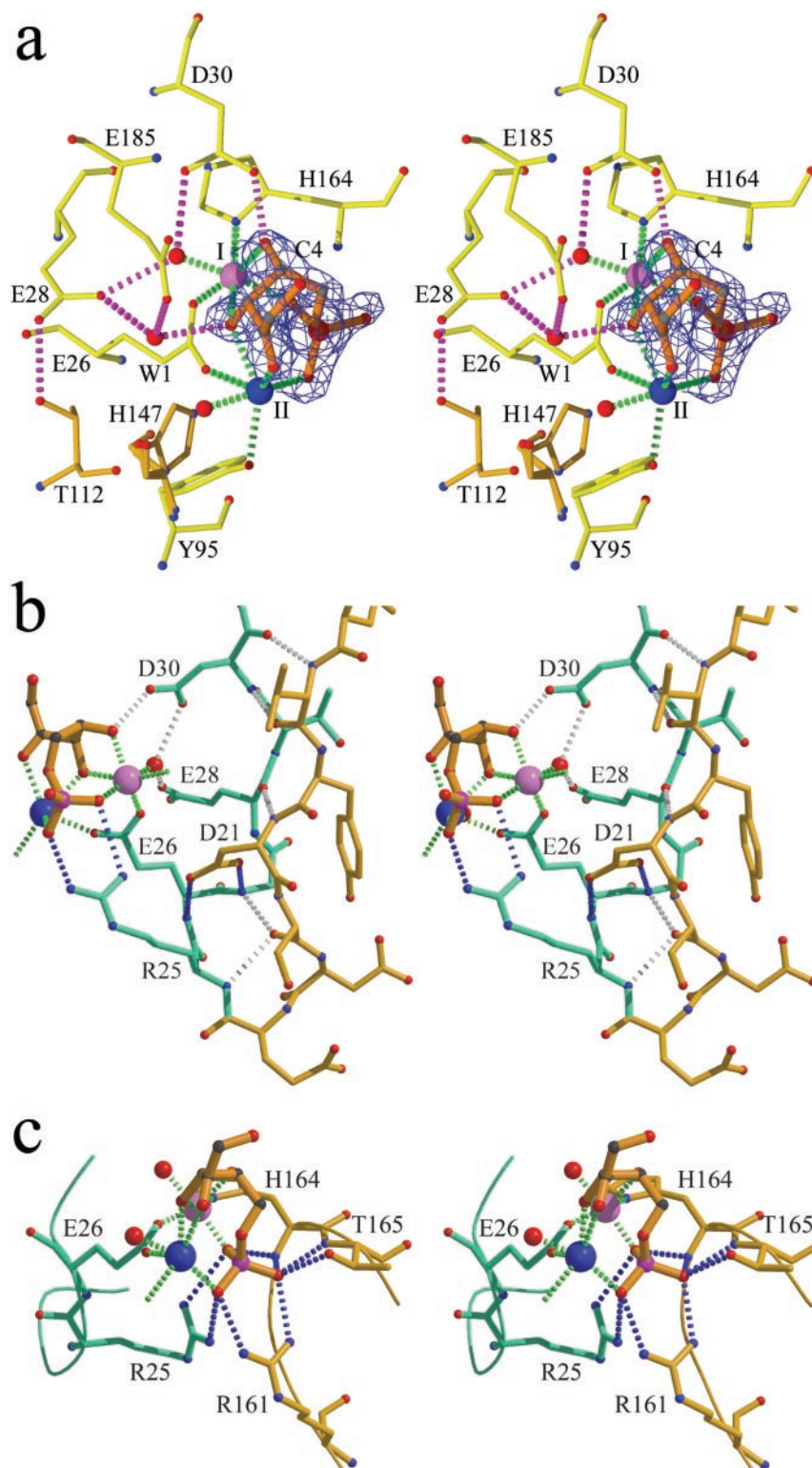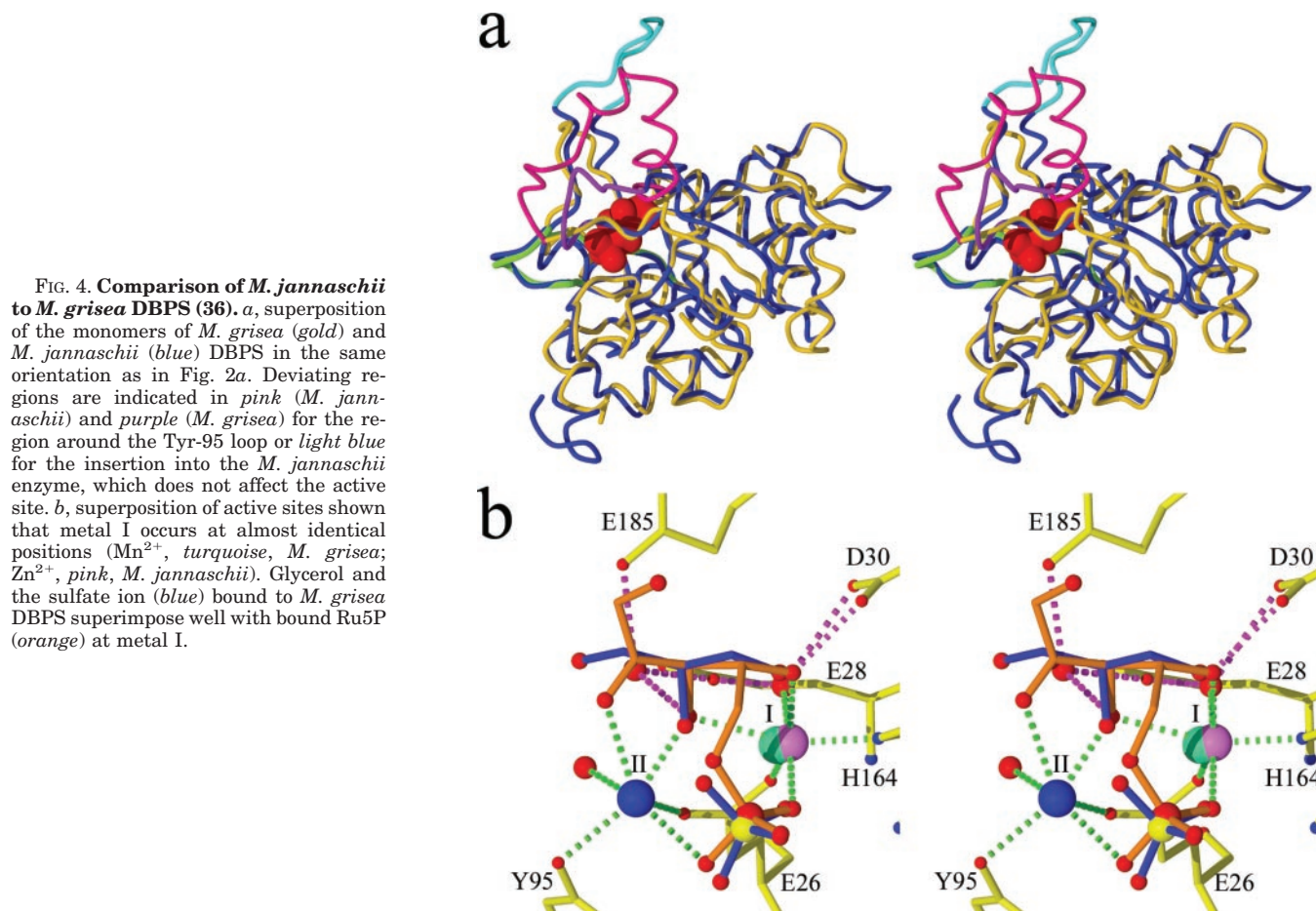
FIG. 3. **Active site architecture.** *a*, binding mode of Ru5P at the dimetal center. The $F_o - F_c$-simulated annealing omit electron density is depicted at a 2.5-σ contour level. *b*, structure of the acidic active site loop. *c*, phosphate binding site.

Zn^{2+} ions. However, at concentrations of 200 mM of the metal ions used for formation of these complexes, four zinc ions were found at the active site. These complexes revealed His-153 and Glu-37 (*M. grisea*) as metal ligands where Glu-37 bridges both metal. Insight into substrate binding has been gained from a fortuitous Mn^{2+}·glycerol·sulfate complex that, however, showed only the histidine-liganded metal I. In that complex metal I binds two hydroxyl groups of glycerol, one oxygen of the sulfate ion, Glu-37, as monodentate ligand and a water molecule.

The present study extends this information to a true substrate complex that was obtained by soaking the monoclinic crystals of the His-147 → Ser mutant of *M. jannaschii* DBPS in the presence of non-functional divalent metal ions, zinc and calcium, at concentrations of 2 and 200 mM, respectively (Fig. 2). In addition, one of the three asymmetric subunits of the orthorhombic crystal form shows a very similar dimetal center with a bound phosphate ion, presumably from incomplete buffer exchange prior to crystallization, whereas the other two monomers obviously have a heterogeneous composition. Be-

FIG. 4. **Comparison of *M. jannaschii* to *M. grisea* DBPS (36).** *a*, superposition of the monomers of *M. grisea* (*gold*) and *M. jannaschii* (*blue*) DBPS in the same orientation as in Fig. 2*a*. Deviating regions are indicated in *pink* (*M. jannaschii*) and *purple* (*M. grisea*) for the region around the Tyr-95 loop or *light blue* for the insertion into the *M. jannaschii* enzyme, which does not affect the active site. *b*, superposition of active sites shown that metal I occurs at almost identical positions (Mn^{2+}, *turquoise*, *M. grisea*; Zn^{2+}, *pink*, *M. jannaschii*). Glycerol and the sulfate ion (*blue*) bound to *M. grisea* DBPS superimpose well with bound Ru5P (*orange*) at metal I.

cause this phosphate ion as well as the phosphate moiety of the substrate also form a ligand to metal II, however, with a slightly larger bond length of about 2.5 Å, compared with 2.2 Å to metal I, it may be speculated that this ligand is required for the full assembly of the dimetal center. It is likely that both metals are only transiently bound to the enzyme, because histidine (His-164) is a relatively unusual ligand for Mg^{2+}, half of the coordination sites of both metals are occupied by the substrate, and a key ligand, Glu-26, bridging both metal sites, is part of the acidic active site loop that is flexible in the absence of substrate.

Does the Substrate Complex Represent a Physiological Conformation?—We have observed two metal ions at the active site, which we have identified as Zn^{2+} (metal I) and Ca^{2+} (metal II). This assignment is based on the crystallographic refinement of temperature factors at 1.7-Å resolution, which should allow discrimination between both options, when full occupancy is assumed (calcium, 20 electrons; zinc, 30 electrons). The refinement yields 28.3 Å^2 (zinc) and 27.3 Å^2 (calcium) for monomer A and 30.8 Å^2 (zinc) and 37.9 Å^2 (calcium) for monomer B, respectively. The orthorhombic crystal form gives values of 28.9 Å^2 (zinc) and 33.7 Å^2 (calcium) in monomer A that show a well ordered dimetal center refined at 2.45-Å resolution. The above assignment yields temperature factors for both metals that are very similar to the surrounding ligands and well within the lower range observed for the protein. In addition, we expect that Zn^{2+} binds with higher affinity to His-164 compensating for its lower concentration. Irrespective of the correctness of this assignment, both potential candidates are enzymatically inactive metals.

Strong support that the observed substrate binding mode at the dimetal center indeed represents a native-like geometry comes from the Mn^{2+}·glycerol·sulfate complex of *M. grisea* DBPS (36). Superposition of the entire monomer (Fig. 4*a*) places the Mn^{2+} ion, the sulfate ion, and both glycerol hydroxyl groups at almost identical positions (Fig. 4*b*) compared with the corresponding components of the substrate complex. The acidic active site loops adopt identical conformations in both complexes. Metal II is absent from the *M. grisea* DBPS complex, however, the dimetal·sulfate complexes show it at very similar positions. In addition, it is well known from numerous examples that divalent metal ions can substitute for one another, in some cases functionally (Mn^{2+} in most cases for Mg^{2+}) in others only structurally. Riboflavin kinase, for example, is active with Mg^{2+} or Zn^{2+} (46) with a rather unusual binding mode of zinc to the backbone carbonyl and side-chain hydroxyl group of a threonine residue (47). In Rubisco, an enzyme that performs a similar enolization reaction in the first step, Ca^{2+} can substitute for Mg^{2+} structurally but not functionally thus allowing the characterization of a substrate complex (48). D-Xylose isomerase requires Mg^{2+}, Mn^{2+}, or Co^{2+}, but Ca^{2+} functions as a strong competitive inhibitor, because it can occupy the Mg^{2+} binding sites (49, 50). In the structure of 3-deoxy-D-*arabino*-heptulosonate 7-phosphate synthase a non-activating lead ion binds to the same four active site ligands as an activating manganese ion (51). We interpret these observations in the sense that zinc and/or calcium ions are able to mediate a native-like binding of the substrate Ru5P to DBPS but are not able to initiate the enolization reaction.

Structure of the Acidic Active Site Loop—The active site loop spans approximately the region from Leu-18 to Val-32 and contains five acidic residues and one arginine. Leu-18, Met-31, and Val-32 anchor the loop in the hydrophobic core of the protein and are part of two β-sheets that include residues up to

FIG. 5. **Structural context of *M. jannaschii* DPBS mutants (30).** Three categories can be distinguished. I, all mutants are inactive (*red*); II, at least some show residual activity (*pink*); and III, all mutants retain considerable activity (*green*).
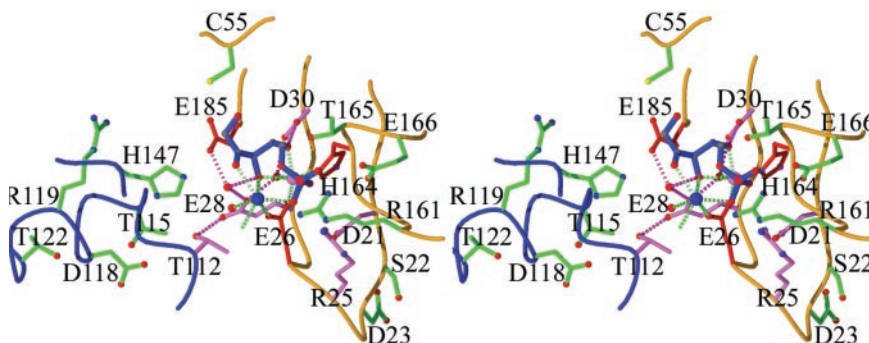
Tyr-20 and from Met-31 onwards (Fig. 3*b*). We observed a total of five copies of the molecule in the absence and presence of substrate for this loop, which shows a variable degree of ordering. Tyr-20, like Ser-22, Asp-23, and Thr-29, points into the solvent. The side chain of Asp-21 forms essential contacts to the backbone amides of Glu-28 (3.0 Å) and Glu-25 (2.7 Å) as well as a salt bridge to Arg-25 (3.3 Å) and thereby stabilizes a loop that includes residues from Ser-22 to Glu-28. Gly-27 seems important, because it allows a sharp kink of the loop. Arg-25 is like the Arg-161 part of the phosphate binding site. Only Glu-26 serves as direct ligand to metal I (Zn^{2+}) and metal II (Ca^{2+}), whereas Glu-28 points into a solvent-filled cavity on the substrate-distant side and contacts a water ligand to this metal. The density for its $C\gamma$ atom is rather weak. Asp-30 is well ordered and points toward the carbohydrate chain of the substrate and at a larger distance toward the same zinc-bound water molecule as Glu-28. The importance for substrate and metal binding of Arg-25, Glu-26, Glu-28, and Asp-30 is reflected by their strict conservation in DBPS proteins. The same is true for Asp-21, which is, however, required for the formation of the loop structure itself.

Structural Context of Active Site Mutants—The active site of *M. jannaschii* DBPS has been explored extensively by mutagenesis (30). Especially conserved residues in close proximity to the bound substrate were each analyzed by a set of mutations, including the most similar amino acid, with respect to size and functionality and functionally dissimilar amino acids. According to this study, active site residues can be grouped into three categories: (i) all mutants are inactive, (ii) at least some mutants show some residual activity, or (iii) mutants retain considerable activity (Fig. 5).

Category I comprises both direct metal ligands, Glu-26 (mutated to Asp, Gln, and Ser) bridging both metals and His-164 (mutated to Asn and Ser) that coordinates metal I. Interestingly, Glu-185 (mutated to Asp, Gln, and Ser) belongs also to this category. It contacts a water molecule hydrogen-bonded to OH3 of the substrate and is the closest side chain to C3, which must be deprotonated in the initial enolization reaction (Fig. 3*a*).

Category II includes Asp-21, Arg-25, Glu-28, Asp-30, and Thr-112. Asp-21 (mutated to Glu, Asn, and Ser) is essential for the conformation of the acidic active site loop, however, the serine mutant shows residual activity. Arg-25 (mutated to Glu and Lys) is part of the phosphate binding site and both mutants have very small residual activity. Glu-28 (mutated to Asp, Gln, and Ser) contacts the same water molecule as Glu-185 next to OH3 of the substrate and a water ligand on metal I. It is additionally fixed by a contact to Thr-112. As only the isosteric glutamine mutation shows residual activity, its stereochemically precise hydrogen-bonding capability seems essential. The effect of the mutation Thr-112Ala is probably mediated by Glu-28, as Thr-112 contributes to the hydrogen bonding pattern of Glu-28 stabilizing its side-chain conformation. It should

be noted that the side chain of Glu-28 shows weak electron density for $C\gamma$ in some subunits, indicating potential flexibility. Asp-30 (mutated to Glu, Asn, and Ser) is in contact to the water ligand on metal I and to OH4 and only the serine mutant shows residual activity.

Category III includes residues of the acidic active site loop (Ser-22 and Asp-23) that point away from the active site, residues near the phosphate binding site (Thr-165, Glu-166, and Arg-161) or residues of the Thr-112 loop (Thr-115, Asp-118, Arg-119, and Thr-122) that are also not in direct vicinity to the active site. Only the high residual activity of Cys-55 (mutated to Ser and Gly) and His-147 (mutated to Ser) mutants are rather surprising, because both residues are in close proximity to the C1 and C2 head groups and were therefore expected to make essential contributions to the enolization step and/or the following dehydration at C1.

Implications for the Catalytic Mechanism—Despite the availability of *E. coli* (34, 35) DBPS without ligands and of the *M. grisea* enzyme in complex with various metals and the fortuitous glycerol complex originating from glycerol as cryoprotectant (36) no reliable information on substrate binding is available up to now. DBPS *M. jannaschii* has been subject to extensive mutagenesis studies that yielded a wealth of information on the functional role of a significant portion of active site residues (30). The present study allows the correlation between the enzymatic activity of these residues and their structural context (Fig. 5). Our results are generally in accordance with those obtained by Liao and colleagues (36) based on the DBPS·Mn^{2+}·glycerol complex, however, with the exception of the contribution of residues Cys-55 and His-147 to dehydration of C1, which is the committed step of the reaction based on mutagenesis data (30). Although the DBPS·Mn^{2+}·glycerol complex shows a water molecule at the site of metal II, their model is also based on the presence of a dimetal center deduced from separate metal soaks.

It has been postulated that the reaction starts with the formation of a 2,3-endiol **1** or **2** (14–16) (Fig. 1) in analogy to the reaction performed by the evolutionary ancient enzyme Rubisco as proposed by Calvin (52) (Fig. 6*a*). The substrate of this enzyme is the very similar ribulose 1,5-diphosphate, which differs only by the additional phosphorylation of position 1, which allows tight fixation of ribulose 1,5-diphosphate in an elongated conformation by two phosphate binding sites as demonstrated by numerous crystal structures (reviewed in Refs. 53 and 54). It should be particularly noted that Ru5P binds to the dimetal center in a very compact conformation and that only the 5-end is anchored by ionic hydrogen-bonding of the 5-phosphate to Arg-25 and Arg-161 as well as by inducer dipolar hydrogen bonding to two backbone amides and the side chain hydroxyl of Thr-165 (Fig. 3*c*). In contrast the 1-hydroxyl group is completely free as this end of Ru5P is only fixed by the contact between O_2 and metal II.

The substrate is clearly bound in its 2-keto form (*Ru5P in*

FIG. 6. **Reactions performed by Rubisco and IspC.** *a*, initial reaction steps of Rubisco. Ribulose 1,5-bisphosphate is converted into an 2,3-enediole that can react with carbon dioxide. Mutants of Rubisco can also undergo β-elimination of the 1 phosphate. *b*, 1-deoxy-D-xylulose 5-phosphate reductoisomerase (IspC) introduces the branched isoprenoid skeleton in the mevalonate-independent pathway (*left*). The complex of IspC with the substrate-like inhibitor fosmidomycin suggests a coordination of the 2-carbonyl and 3-hydroxyl groups of 1-deoxy-D-xylulose 5-phosphate by Mn^{2+} supporting the 1,2-sigmatropic reaction.
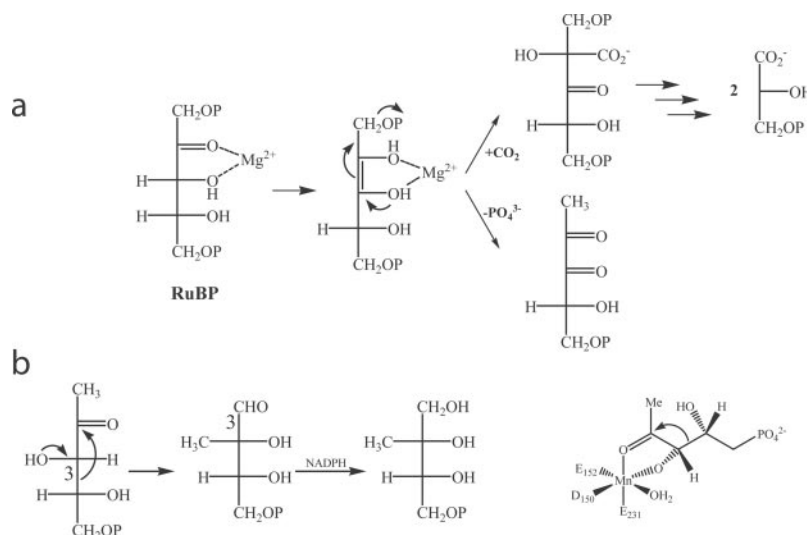

Fig. 1); therefore, enediol formation is obviously not supported by Zn^{2+} and/or Ca^{2+}, which are presumably not hard enough as Lewis acids to do so, freezing the reaction in the substrate complex state. The proton on C3 has to be removed for enolization. The only side chain in close proximity to C3 is that of Glu-185 (3.5 Å to Oε2). The next closest residue Asp-30 is significantly further away (4.9 Å to Oδ1) and hydrogen bonded to a water molecule at metal I (3.0 Å) and O4 of Ru5P (Fig. 3a). Therefore, Glu-185, indispensable for catalysis (30), is the only available residue that might directly promote deprotonation of C3. In our complex, water W1 forms a hydrogen bond to O3 and two carboxylates of Glu-28 and Glu-185, respectively, therefore O3 might still be protonated in our substrate complex. However, it is generally accepted that stabilization of the enolate species either by metals or strong hydrogen bonds is the main source of the activation free-energy barrier reduction as shown for glyoxalase I, triosephosphate isomerase, and ketosteroid isomerase (55). This nevertheless does not rule out a substantial contribution of Glu-185 to enolization by the deprotonation of C3, which is supported by the enolate-stabilizing effect of two metal ions contacting O3. Because the 2-oxygen of Ru5P is coordinated to metal II a *cis*-geometry for the 2,3-enediol will result.

In Rubisco the enolization is supported by a single Mg^{2+} ion corresponding to metal II in DBPS that coordinates O2 and O3 of RuBP (Fig. 6a). The nearby carbamate group on Lys-201 that coordinates this single Mg^{2+} ion in addition to Asp-208 and Glu-204 (numbering of spinach Rubisco) is discussed as base abstracting the proton from C3 and shuffling protons between O3 and O2. Due to the elongated conformation of RuBP none of both phosphates contacts the single Mg^{2+} ion.

The next step involves dehydration at C1 and formation of a 2-enolate, which requires protonation of OH1 as leaving group. The resulting enediol **3** is supposed to tautomerize to form the 2,3-diketo compound **4** (1-deoxy-D-*glycero*-2,3-pentodiulose 5-phosphate) with both oxygen atoms presumably still bound to metals I and II. The dehydration at C1 is reminiscent of β-elimination of phosphate from *cis*-enediol phosphates. It is a common side reaction that has been described as rapid in free solution for triosephosphates (56), which affects the triosephosphate isomerase-catalyzed reaction. β-Elimination of the 1-phosphate is also known as unproductive side reaction of both ene-diolates occurring during the reaction of Rubisco. This process is significant in native Rubisco for the second enediol of the hydrated six-carbon aci-intermediate, accounting for at least 0.7% of the turnover, which produces pyruvate after

cleavage of the C-2/C-3 bond (57). β-Elimination of the 1-phosphate from the initial 2,3-enediol (Fig. 6a) is efficiently suppressed by freezing the geometry of RuPB in a conformation where the bridging oxygen of P1 is in plane with C1, C2, and C3 but can be enhanced in some active site mutants affecting the 1-phosphate binding site (58, 59). This reaction yields 1-deoxy-D-glycero-2,3-pentodiulose 5-phosphate, the same 2,3-diketo intermediate **4** is postulated for DPBS (Fig. 1).

Because water is worse than phosphate as a leaving group, this elimination process may be significantly slower in free solution than the β-elimination of phosphates and will have to be supported by the enzyme. Besides the hydrophobic residues Phe-101 (4.3 Å to Cζ), Leu-151 (4.8 Å to Cδ2), Leu-53 (4.7 Å to Cδ1) the closest residues to C1 are Cys-55 (3.8 Å to Sγ) and His-147 (modeled at ~4.0 Å to Nε) in the substrate complex. Both His-147 and Cys-55 could be involved as proton sources for both the dehydration at C1 and following proton shuffling between O2 and O3. It should be noted that the side chain of His-147 is fixed by a hydrogen bond to Asn-106 and not activated in an Asp-99 to His-136 dyad like the corresponding His-136 in the *M. grisea* enzyme (36). Surprisingly, the mutants Cys-55 → Ser, Cys-55 → Gly, and His-147 → Ser retain about 30, 13, and 12% of wild type V_{max}, respectively (30), which indicates a geometric function. Especially, histidine residues are often implicated in proton transfer reactions when found at active sites. The prime contribution of His-147 and/or Cys-55 in DBPS could therefore be the optimal alignment of OH1 for elimination and to a lesser extent its protonation. A major driving force may be again stabilization of the conjugated enolate system in **3** by metal I and II.

1-Deoxy-D-glycero-2,3-pentodiulose 5-phosphate **4** is fairly stable in solution and can be isolated by anion-exchange chromatography from the reaction mixture of Rubisco mutants (58). It can be speculated that O2, O3, and O4 remain bound at the dimetal center also during later steps of the reaction like suggested for Rubisco. In that case, the electron-withdrawing effect of the 2-keto group combined with metal coordination is expected to increase the electrophilic character of C3 significantly. This will promote migration of the nearby C5 to C3. It should be particularly noted that this sigmatropic shift is supported by the compact geometry of the substrate induced by coordination of O3, O4, and the phosphate moiety by metal I (Fig. 3a). In the resulting branched carbon skeleton in **5**, C4 is present as a formyl group.

The skeletal rearrangement performed by DBPS bears some resemblance to those performed by ketol acid reductoisomer-

ase (60) and 1-deoxy-D-xylulose 5-phosphate reductoisomerase (IspC) (61) that establish the branched carbon skeletons of some amino acids and of isoprenoids, respectively. For the latter, a molecular mechanism based on the complex between the substrate-like inhibitor fosmidomycin and IspC in the presence on manganese was recently suggested (62) (Fig. 6*b*). In that model, the 2-carbonyl and 3-hydroxyl groups of 1-deoxy-D-xylulose 5-phosphate are coordinated to manganese increasing the electrophilic character of the 2-carbonyl group, which can be attacked by C4 as nucleophile resulting in a similar 1,2-shift.

In a final step the formyl group generated from C4 (**5**) is proposed to be hydrated (**6**) for its elimination as formate. Aldehyde hydrates are generally unstable but nevertheless occur transiently in a number of reactions like that performed by alcohol dehydrogenase (63). They can even be stabilized like in arylsulfatases where a Ca^{2+}-coordinated formyl hydrate originating from a conserved cystein or serine residue by post-translational modification has been observed at the active site (64). The postulated formyl hydrate **6** could be stabilized by metal I in a similar way. It has been suggested that the water ligand of metal I may serve for formyl hydrate formation (36), which is analogous to the mechanism suggested for alcohol dehydrogenase. In the final step the C4 group is eliminated in a retro-aldol reaction leading to the enediole **7** and finally to the product 3,4-dihydroxy-2-butanone 4-phosphate DHBP.

The reaction sequence outlined here requires changes in geometry accompanied by alteration of the hybridization state of C2 and C3 and even migration of C5. These may be accommodated by a slight distortion of the metal coordination without requiring detachment of O2, O3, or O4. Especially the coordination sphere of metal II shows certain variability in various copies of the molecule supporting this idea. It has been suggested that the 1,2-hydride shift in xylose isomerase is associated with a breathing motion of a similar dimetal center (65).

CONCLUSION

We described, for the first time, the complex a 3,4-dihydroxy-2-butanone 4-phosphate synthase (DBPS) with its substrate ribulose 5-phosphate complexed with divalent metal ions that allows the detailed analysis of metal-mediated enzyme substrate interactions. Formation of the 2,3-enediol of ribulose in a metal-dependent way starting with geometry as described by the present crystallographic study is sufficient to initiate chemical reactions of the carbohydrate. In Rubisco the formation of the 2,3-endiol of the similar substrate ribulose-1,5-diphosphate converts C2 into a nucleophile that can react either with carbon dioxide or molecular oxygen but that is also prone to β-elimination that must be suppressed. In DBPS a similar β-elimination of water from the 2,3-enediol intermediate of ribulose 5-phosphate is probably used to facilitate cleavage of the C1–O1 bond leading to 2,3-diketone. The compact conformation supports the sigmatropic skeletal rearrangement reaction that finally yields formate and 3,4-dihydroxy-2-butanone 4-phosphate. The fact that residues of the second coordination sphere of the substrate in DBPS have a significantly reduced influence on the reaction strongly argues that the first coordination sphere is sufficient to initiate the reaction, and the second coordination sphere is probably involved in avoiding unproductive side reactions of highly reactive intermediates as observed for wild-type or mutant Rubisco.

REFERENCES

1. Müller, F. (1992) *Chemistry and Biochemistry of Flavoenzymes*, Vol. 3, CRC Press, Boca Raton, FL
2. Sancar, A. (1994) *Biochemistry* **33**, 2–9
3. Salomon, M., Eisenreich, W., Dürr, H., Schleicher, E., Knieb, E., Massey, V., Rüdiger, W., Müller, F., Bacher, A., and Richter, G. (2001) *Proc. Natl. Acad. Sci. U. S. A.* **98**, 12357–12361
4. Briggs, W. R., and Huala, E. (1999) *Annu. Rev. Cell Dev. Biol.* **15**, 33–62
5. O'Kane, D. J., and Prasher, D. C. (1992) *Mol. Microbiol.* **6**, 443–449
6. Lee, J. (1985) in *Chemiluminescence and Bioluminescence* (Burr, J. G., ed) pp. 401–437, Marcel Dekker, Inc., New York
7. Meighen, E. A. (1991) *Microbiol. Rev.* **55**, 123–142
8. Meighen, E. A. (1993) *FASEB J.* **7**, 1016–1022
9. Bornemann, S. (2002) *Nat. Prod. Rep.* **19**, 761–772
10. Bacher, A., Eberhardt, S., and Richter, G. (1996) in *Escherichia and Salmonella* (Neidhardt, F. C., Ingraham, J. L., Low, K. B., Magasanik, B., Schaechter, M., and Umbarger, H. E., eds) Vol. 1, 2nd Ed., pp. 657–664, 2 vols., Washington, D. C.
11. Bacher, A., Eberhardt, S., Fischer, M., Kis, K., and Richter, G. (2000) *Annu. Rev. Nutr.* **20**, 153–167
12. Bacher, A., Eberhardt, S., Eisenreich, W., Fischer, M., Herz, S., Illiaronov, B., Kis, K., and Richter, G. (2001) in *Biosynthesis of Riboflavin: Vitamins and Hormones* (Begley, T., ed) p. 61, Academic Press, New York
13. Young, D. W. (1986) *Nat. Prod. Rep.* **3**, 395–419
14. Volk, R., and Bacher, A. (1988) *J. Am. Chem. Soc.* **110**, 3651–3653
15. Volk, R., and Bacher, A. (1990) *J. Biol. Chem.* **265**, 19479–19485
16. Volk, R., and Bacher, A. (1991) *J. Biol. Chem.* **266**, 20610–20618
17. Fischer, M., Haase, I., Kis, K., Meining, W., Ladenstein, R., Cushman, M., Schramek, N., Huber, R., and Bacher, A. (2003) *J. Mol. Biol.,* **326**, 783–793
18. Foor, F., and Braun, G. M. (1975) *J. Biol. Chem.* **250**, 3545–3551
19. Burrows, R. B., and Brown, G. M. (1978) *J. Bacteriol.* **136**, 657–667
20. Harzer, G., Rokos, H., Otto, M. K., Bacher, A., and Ghisla, S. (1978) *Biochim. Biophys. Acta* **540**, 48–54
21. Hollander, I., Brown, G. M. (1979) *Biochem. Biophys. Res. Commun.* **89**, 759–763
22. Nielsen, P., and Bacher, A. (1981) *Biochim. Biophys. Acta* **662**, 312–317
23. Neuberger, G., and Bacher, A. (1986) *Biochem. Biophys. Res. Commun.* **139**, 1111–1116
24. Richter, G., Ritz, H., Katzenmeier, G., Volk, R., Kohnle, A., Lottspeich, F., Allendorf, D., and Bacher, A. (1993) *J. Bacteriol.* **175**, 4045–4051
25. Richter, G., Fischer, M., Krieger, C., Eberhardt, S., Lüttgen, H., Gerstenschläger, I., and Bacher, A. (1997) *J. Bacteriol.* **179**, 2022–2028
26. Scheuring, J., Kugelbrey, K., Weinkauf, S., Cushman, M., Bacher, A., and Fischer, M. (2001) *J. Org. Chem.* **66**, 3811–3819
27. Plaut, G. W. E. (1960) *J. Biol. Chem.* **235**, 41–42
28. Plaut, G. W. E., Smith, C. M., and Alworth, W. (1974) *Annu. Rev. Biochem.* **43**, 899–922
29. Wacker, H., Harvey, R. A., Winestock, C. H., and Plaut, G. W. E. (1964) *J. Biol. Chem.* **239**, 3493–3497
30. Fischer, M., Römisch, W., Schiffmann, S., Kelly, M., Oschkinat, H., Steinbacher, S., Huber, R., Eisenreich, W., Richter, G., and Bacher, A. (2002) *J. Biol. Chem.* **277**, 41410–41416
31. Peach, C., Pierce, J., McCurry, S. D., and Tolbert, N. (1978) *Biochem. Biophys. Res. Commun.* **83**, 1084–1092
32. Pierce, J., Tolbert, N. E., and Darker, R. (1980) *Biochemistry* **19**, 934–942
33. Pierce, J., Andrews, T. J., and Lorimer, G. (1986) *J. Biol. Chem.* **261**, 10248–10256
34. Liao, D.-I., Calabrese, J. C., Wawrzak, Z., Viitanen, P. V., and Jordan, D. B. (2001) *Structure* **9**, 11–18
35. Kelly, M. J., Ball, L. J., Krieger, C., Yu, Y., Fischer, M., Schiffmann, S., Schmieder, P., Kuhne, R., Bermel, W., Bacher, A., Richter, G., and Oschkinat, H. (2001) *Proc. Natl. Acad. Sci. U. S. A.* **98**, 13025–13030
36. Liao, D.-I., Zheng, Y.-J., Viitanen, P. V., and Jordan, D. B. (2002) *Biochemistry* **41**, 1795–1806
37. CCP4 (1994) *Acta Crystallogr. Sect. D Biol. Crystallogr.* **50**, 760–763
38. Otwinowski, Z., and Minor, W. (1997) *Methods Enzymol.* **276**, 307–326
39. Sheldrick, G. M., Dauter, Z., Wilson, K. S., Hope, H., and Sieker, L. C. (1993) *Acta Crystallogr.* **D49**, 18–23
40. Jones, T. A. (1992) in *Molecular Replacement* (Dodson, E. J., Gover, S., and Wolf, W., eds) pp. 91–105, SERC Daresbury Laboratory, Warrington, UK
41. Turk, D. (1992) *Weiterentwicklung eines Programms für Molekülgraphik und Elektronendichte-Manipulation und seine Anwendung auf verschieden Protein-Strukturaufklärungen*, Ph.D. thesis, Technische Universität München, München, Germany
42. Brunger, A. T., Adams, P. D., Clore, G. M., DeLano, W. L., Gros, P., Grosse-Kunstleve, R. W., Jiang, J. S., Kuszewski, J., Nilges, M., Pannu, N. S., Read, R. J., Rice, L. M., Simonson, T., and Warren, G. L. (1998) *Acta Crystallogr. Sect. D Biol. Crystallogr.* **54**, 905–921
43. Brünger, A. (1992) *Nature* **355**, 472–475
44. Ramachandran, G. N., and Sasisekharan, V. (1968) *Adv. Protein. Chem.* **23**, 283–437
45. Laskowski, R. A., MacArthur, M. W., Moss, D. S., and Thornton, J. M. (1993) *J. Appl. Crystallogr.* **26**, 283–291
46. Merrill, A. H., and McCormick, D. B. (1980) *J. Biol. Chem.* **255**, 1335–1338
47. Bauer, S., Kemter, K., Bacher, A., Huber, R., Fischer, M., and Steinbacher, S. (2003) *J. Mol. Biol.* **326**, 1463–1473
48. Taylor, T. C., and Andersson, I. (1997) *J. Mol. Biol.* **265**, 432–444
49. Callens, M., Tomme, P., Kersters-Hilderson, H., Cornelis, W., Vangrysperre, W., and De Bruyne, C. K. (1988) *Biochem. J.* **250**, 285–291
50. Collyer, C. A., Henrick, K., and Blow, D. M. (1990) *J. Mol. Biol.* **212**, 211–235
51. Wagner, T., Shumilin, I. A., Bauerle, R., and Kretsinger, R. H. (2000) *J. Mol. Biol.* **301**, 389–399
52. Calvin, M. (1954) *Fed. Proc.* **13**, 697

53. Cleland, W. W., Andrews, T. J., Gutteridge, S., Hartman, F. C., and Lorimer, G. H. (1998) *Chem. Rev.* **98,** 549–561
54. Spreitzer, R. J., and Salvucci, M. E. (2002) *Annu. Rev. Plant Biol.* **53,** 449–475
55. Feierberg, I., and Aqvist, J. (2002) *Theor. Chem. Acc.* **108,** 71–84
56. Richard, J. P. (1984) *J. Am. Chem. Soc.* **106,** 4926–4936
57. Andrew, T. J., and Kane, H. J. (1991) *J. Biol. Chem.* **266,** 9447–9452
58. Larimer, F. W., Harpel, M. R., and Hartman, F. C. (1994) *J. Biol. Chem.* **269,** 1114–11120
59. Morell, M. K., Paul, K., O'Shea, N. J., Kane, H. J., and Andrews, J. T. (1994) *J. Biol. Chem.* **272,** 5445–5451
60. Dumas, R., Biuo, V., Halgand, F., Douce, R., and Duggleby, R. G. (2001) *Acc. Chem. Res.* **34,** 399–408
61. Takahashi, S., Kuzuyama, T., Watanabe, H., and Seto, H. (1998) *Proc. Natl. Acad. Sci.* **95,** 9879–9884
62. Steinbacher, S., Kaiser, J., Eisenreich, W., Huber, R., Bacher, A., and Rohdich, F. (2003) *J. Biol. Chem.* **278,** 18401–18407
63. Olson, L. P., Luo, J., Almarsson, O., and Bruice, T. C. (1996) *Biochemistry* **35,** 9782–9791
64. Boltes, I., Czapinska, H., Kahnert, A., von Bulow, R., Dierks, T., Schmidt, B., von Figura, K., Michael A. Kertesz, M. A., and Uson, I. (2001) *Structure* **9,** 483–491
65. Garcia-Viloca, M., Alhambra, C., Truhlar, D. G., and Gao, J. (2002) *J. Am. Chem. Soc.* **124,** 7268–7269